Road salt compromises functional morphology of larval gills in populations of an amphibian

Running title: Salt alters amphibian gill structure

Keywords: osmoregulation; osmotic stress; pollution; road effects; road salt; secondary salinization

Manuscript type: Primary research

The manuscript contains a table, a single panel figure, four multi-panel figures, and a supplemental table.

Richard V. Szeligowski[1]
Jules A. Scanley[2]
Christine C. Broadbridge[2]
Steven P. Brady[1]

[1]Biology Department, Southern Connecticut State University. New Haven, CT 06515.
[2]Center for Nanotechnology, Connecticut State Colleges and Universities. New Haven, CT 06515.

Corresponding Author:

Richard Szeligowski

Richard.szeligowski@yale.edu

Summary Statement:

Chronic road salt exposure alters the functional morphology of gills in larval amphibians, potentially compromising osmoregulation, feeding, and respiration.

Abstract

Throughout much of the world, winter deicing practices have led to secondary salinization of freshwater habitats, where numerous taxa are vulnerable to elevated salinity. Many amphibians are of particular concern because of their permeable skin and reliance on small ponds and pools, where salinity levels can be high. The early life-history stages of amphibians that develop in these habitats are especially sensitive to salt exposure. Larvae developing in salt-polluted environments must osmoregulate through ion exchange in gills. While salt-induced changes to the physiology of ion exchange in amphibian gills is generally understood, functionally relevant changes in gill morphology remain poorly described. Yet the structure of gills should be an important component affecting their ionoregulatory capacity, for instance in terms available surface area. Larval amphibian gills also play critical roles in gas exchange and foraging. Thus, changes in gill morphology due to salt pollution potentially affect not only osmoregulation, but also respiration and feeding. Here, we used a chronic exposure experiment to quantify the effect of salinity on larval gill morphology in populations of the wood frog (*Rana sylvatica*). We measured a suite of morphological traits on gill tufts, where ionoregulation and gas exchange occur, and on gill filters, which are used in feeding. Larvae raised in high salinity conditions had gill tufts with lower surface area to volume ratio, while epithelial cells on these tufts were less circular but occurred at higher densities. Gill filters showed increased spacing, which can potentially reduce their efficiency in filtering food particles. Together, these changes seem likely to diminish the ionoregulatory and respiratory capacity of gill tufts, and compromise feeding functionality of gill filters. Thus, a singular change in the aquatic environment from a widespread pollutant has the potential to generate a suite of consequences via changes in gill morphology. Critically, this suite of negative effects is likely most detrimental in salinized environments, where ionoregulatory demands are higher, which in turn should increase respiratory demands along with energy acquisition demands through foraging.

Introduction

Salt pollution: a widespread problem for freshwater organisms

Freshwater habitats are becoming salinized by pollution from human activities including industrial processes, mining effluent, agricultural runoff, and most substantially, road salt used for de-icing (Lauer et al. 2016; Kaushal et al., 2005; Dugan et al., 2017; Maloney et al., 2017). Road salt applied to roadways, driveways, walkways, and parking lots runs off into adjacent habitats and/or stormwater infrastructure, and much of this salt is carried into surface waters. For instance, one estimate suggests that about 70% of lakes in the North American Lakes Region are polluted by road salt, and that if current salting practices continue, chloride pollution levels in many lakes will exceed the EPA's water quality criterion 2050 (Dugan et al., 2017).

Elevated salinity in freshwater habitats spurs a suite of negative effects across biological levels, from genetic to ecosystem (Hintz et al., 2017; Gibbons et al., 2018; Merrick and Searle, 2019; Venâncio et al., 2019). For many freshwater taxa, salt pollution causes numerous sublethal effects, including changes in foraging and anti-predator behavior (Hall et al., 2017); changes in life history traits (Faulkner et al., 2019); and increased malformations (Brady, 2013; Hopkins et al., 2013; Alam et al., 2020). Salt can also be directly toxic (Sanzo and Hecnar, 2006; Karraker et al., 2008; Mahrosh et al., 2014). Together, these impacts can lead to loss of genetic diversity, population declines, and changes in community composition (Van Meter and Swan, 2014; Castillo et al., 2018), which collectively can modify ecosystem function (Schuler et al., 2017). Salt pollution also affects biogeochemical cycles, and these changes can scale up through food webs (Judd et al., 2005). For instance, salt pollution increases nitrogen and carbon export in streams (Reviewed in Hintz and Relyea, 2019) while plant and zooplankton richness have both been shown to decline in freshwater habitats polluted by salt (Richburg et al., 2001; Gutierrez et al., 2018).

While many freshwater taxa are affected by salt pollution, amphibians are of particular concern in part because of ongoing global population declines (Green et al., 2020). Although a subset of amphibians is tolerant of saline conditions (Hopkins and Brodie, 2015), many are considered vulnerable to increased salinization because they have narrow osmotic ranges (Chinathamby et al., 2006; Sanzo and Hecnar, 2006; Brady, 2013), possess highly permeable skin (Pough, 2007), and rely on freshwater habitats for reproduction, development, and dwelling (Vences and Köhler, 2008). While even modest increases in salt can be detrimental (Venâncio et al., 2019), concentrations can become especially high in shallow and/or temporary habitats (e.g., vernal

pools), which many amphibians require to complete their lifecycle (Semlitsch and Skelly, 2007). Consequences of exposure to secondary salinization in amphibians include osmotic stress (Gomez-Mestre et al., 2004) and increased energy allocated to osmoregulation (Peña-Villalobos et al., 2016); increased risk of predation (Denoël et al., 2010); behavioral changes including reduced swim performance (Squires et al., 2008) and reduced foraging activity (Hall et al., 2017); decreased abundance (Albecker and McCoy, 2017); lower larval survival rates and ultimately, population size (Karraker et al., 2008).

Osmoregulation in amphibians

Many amhibians have complex life cycles (Semlitsch and Skelly, 2007), and the negative effects of salt exposure tend to be most severe during early stages of development as embryos and larvae (Gomez-Mestre et al., 2004; Alexander et al., 2012; C.S. Wu et al., 2014; Park and Do, 2020). In anuran larvae, gills are the primary site of ionoregulation—a key mode of osmoregulation in which ions are exchanged between internal and external environments to maintain internal ion concentrations, especially Na^+ and Cl^- (Alvarado and Moody, 1970; Dietz and Alvarado, 1974). For amphibians in typical (unpolluted) freshwater habitats, the tendency is for ions to be lost to the external environment. Osmoregulation for amphibians in these environments requires actively pumping ions in through gill epithelium into systemic plasma (Boonkoom and Alvarado, 1971). The primary mechanism responsible for ion exchange is the Na^+/K^+ ATPase ion pump (NKA). NKA is a transmembrane pump found in all animals that maintains body fluid homeostasis by exporting 3 Na^+ ions while importing 2 K^+ ions per ATP molecule against their respective concentration gradients (Skou, 1957; Pivovarov et al., 2019; Fig. 1). NKA-mediated osmoregulation operates via passive influx of Na^+ from the external environment into an apical epithelial cell. From there, NKA actively transports Na^+ ions into the Na^+-rich plasma while exchanging K^+ from the plasma into the cytosol, where K^+ concentrations are higher. K^+ ions exit the cytosol back into the plasma via passive membrane channels, which creates an electric potential between the external environment and the plasma, leading to passive influx of Cl^- ions and creating a hyperosmotic internal environment (Campbell et al., 2012).

Anuran gills are thought to function much like those of teleosts (Ultsch et al., 1999) in that NKA is highly expressed in mitochondrion-rich cells (MRCs) in the gill epithelium, where MRCs function as the primary mechanism of ionoregulation (Hwang and Lee, 2007). When freshwater amphibian species experience osmoregulatory challenges through salinization, they must prevent water loss by increasing ion absorption, thereby maintaining a hyperosmotic internal

environment (Gomez-Mestre et al., 2004). Bernabò et al. (2013) found that larvae of the common toad (*Bufo bufo*) and Balearic green toad (*Bufo balearicus*) increased NKA abundance in response to increasing salinity, presumably to maintain a hyperosmotic internal environment and prevent water loss. Euryhaline (i.e., salinity tolerant) amphibians such as the Indian rice frog (*Fejervarya limnocharis*) seem to utilize the same strategy for osmoregulation, although the specific mechanisms that allow increased salinity tolerance are not fully understood. Wu *et al.* (2014) found that crab-eating frog (*Rana cancrivora*) tadpoles acclimated to salinity levels corresponding to 15,700 µS/cm had a six-fold increase in NKA abundance when compared to those raised in 4,000 µS/cm water. Although crab-eating frog tadpoles can survive in full strength seawater after acclimation (Gordon and Tucker, 1965), Hsu *et al.* (2012) found that metamorphosis occurred in only 40% of tadpoles in salinity levels corresponding to 60% seawater (30,000 µS/cm) after salinity acclimation.

Toward improved understanding of gill morphology in osmoregulation

In contrast to our knowledge of *physiological* mechanisms underpinning osmoregulation in larval amphibians, we have limited understanding of the functional role of gill morphology, and how it might be affected by salt exposure. Yet changes in gill morphology are important adaptations in fish that transition between freshwater and seawater (Uchida et al., 1996; Hiroi et al., 1999), and thus might be important in freshwater amphibians exposed to salt. Limited, primarily qualitative insights from an acute exposure experiment show that high salinity can modify gill morphology in larvae of the green toad (*Bufo balearicus*) and common toad (*Bufo bufo*) (Bernabò et al., 2013). Specifically, gill tufts became “dehydrated” and “invaginated” in larvae exposed to 12,700 µS/cm. For larvae exposed to 15,000 µS/cm, hyperplasia was observed in pavement cells, which play a limited role in ion exchange (Wilson, 2011). While these qualitative insights are important, they were based on short-term exposure to salt concentrations far above those found in most secondarily-salinized freshwater habitats. Thus, a quantitative assessment of morphology, based on chronic exposure to ecologically relevant salinity levels for pollution is critically needed.

Changes in larval amphibian gill filter morphology could also affect gas exchange and therefore respiration. And because gills are also important structures for larval feeding, salt-induced morphological changes may hamper foraging efficiency. For instance, if gill morphology becomes less well suited to trapping food particles, larvae should experience relative increases in foraging demand. Conceivably, these various effects could be multiplicative: increased demands for ionoregulation in salt-polluted environments could change gill morphology in ways

that reduce efficiency for ionoregulation and gas exchange, driving energetic demands higher. At the same time, reduced foraging efficiency could further increase energetic demands. Thus, any changes in gill morphology have the potential to generate a cascade of effects on amphibian physiology and fitness.

Here, we begin exploring these potential effects by quantifying changes in gill morphology in populations of the wood frog (*Rana sylvatica*). We raised wild-collected embryos in low and high salinity conditions, from early embryonic stages until nearing metamorphosis. We used scanning electron microscopy to image and quantify changes in gill morphology in response to salinity. We hypothesized that increased salinity would alter gill morphology, particularly at the gill tufts and filters. These sites, respectively, are where most osmoregulation occurs via NKA activity (Brunelli et al., 2004), and where food particles are filtered for feeding (Seale and Wassersug, 1979). We predicted that salt would modify gill morphology in ways that compromise ionoregulatory capacity, gas exchange, and feeding.

Methods

Natural History and larval gill function

Wood frogs are found throughout the northern ranges of North America, from the southern Appalachian Mountains through Canadian and Alaskan forests in habitats including tundra, deciduous and coniferous forests, marshes, and grasslands (Green et al., 2014). Wood frog breeding is seasonal. In our study region in the northeastern U.S., adults migrate from upland terrestrial habitat to nearby small, shallow, and often temporary ponds, typically during the first warm rain of early spring following hibernation. Breeding is generally explosive, occurring over a 1-2 week period in each pond. Each female lays one clutch as a single egg masses containing about 1,000 eggs, which are fertilized externally during amplexus. Eggs develop for about 2-3 weeks before hatching, after which time larvae (i.e., tadpoles) develop for about two months before metamorphosing into terrestrial juveniles.

Among amphibians, the wood frog stands out as having a particularly puzzling response to salt exposure. Not surprisingly, this species shows a variety of negative responses to salt pollution and roadside dwelling including many of the known negative effects associated with salt exposure, such as direct mortality and increased malformation in embryos and larvae (Karraker et al., 2008; Brady, 2013) as well as reduced growth rates and increased developmental variance (Brady, 2013; Dananay et al., 2015). However, reciprocal transplants and common garden experiments reveal that aquatic-stage wood frogs from salt-polluted roadside ponds are

more sensitive to road salt and roadside conditions than nearby populations from unpolluted ponds (Brady, 2013; 2017). These findings suggest that roadside populations might have recently evolved lower tolerance to salt than individuals from unpolluted populations, consistent with 'local maladaptation' processes (Brady et al., 2019). Alternatively, this pattern might reflect a fitness tradeoff between aquatic- and terrestrial-stage frogs, for instance if lower salt tolerance is correlated with adult lifetime reproductive success. In either case, we speculate that the survival disadvantage in roadside populations might arise through effects on gill morphology.

During larval development, the primary site of respiration changes. Prior to feeding stage - Gosner (Gosner, 1960) stage 25 - respiration occurs primarily via cutaneous diffusion and the limited activity of external gills before transitioning to gas exchange in a bilateral pair of internal gills (Feder and Burggren, 1992; Brunelli, 2004). Each internal gill contains three prominent branchial arches that originate in the rostral end of the gill, extending caudally. A reduced fourth branchial arch lateral to the first three arches is present in some species but has decreased tuft density and filter plate size (McIndoe and Smith, 1984; Brunelli et al., 2004). Gill tufts are the primary site of gas exchange (McIndoe and Smith, 1984; Brunelli et al., 2004), protruding ventrally from the branchial arch. Each tuft has numerous smaller structures that split from the main body (hereafter 'tuft branches'). A cartilaginous filter plate protrudes dorsally from the branchial arch (McIndoe and Smith, 1984), and rows of gill filters extend laterally from the filter plate, with main folds running ventrodorsally in a zigzag pattern (McIndoe and Smith, 1984). Secondary folds branch from the main folds at corners, often continuing the zigzag pattern of main folds, tertiary folds branch away from secondary folds at their corners, often forming a rectangular filter niche with the main and secondary folds (McIndoe and Smith, 1984). We termed points where folds changed directions, branched into other folds, or terminated 'nodes'.

Gill filters function as a screen for food particulates as water travels over them towards the tufts (Feder et al., 1984; McIndoe and Smith, 1984; Brunelli et al., 2004). Both gill tufts and filters play roles in ionoregulation. However, tufts seem to play a greater part than filters in this capacity. For instance, Bernabò et al. (2013) showed NKA is more strongly expressed in gill tufts than filters in both common toad and Balearic green toad gills, although NKA expression increased in tufts and filters for both species when exposed to salt levels between 5%-25% sea water.

Embryo collection and rearing

220 We collected egg masses from six natural ponds in Norwich, VT during the breeding season in
221 April 2019. To represent a range of populations, we sampled egg masses from three salt-
222 polluted 'roadside' ponds located within 10 m of a paved road and three unpolluted 'woodland'
223 ponds, which were located at least 500 m from any road. From each pond, a cluster of
224 approximately 20 embryos were removed from each of five egg masses. Selection of egg
225 masses and embryo groups was haphazard. Embryo clusters were placed in plastic 700 ml
226 (16.5 x 7.5 x 12.5 cm) containers filled with natal pond water and were immediately transported
227 to the lab in New Haven, CT where they were stored at 4˚C for 24 hours until the start of the
228 chronic salt-exposure experiment.

229 Four salinity treatments were prepared using aged, conditioned tap water and NaCl road salt
230 obtained from the Connecticut Department of Transportation. Embryos were exposed to one of
231 four treatments: 275 µS/cm (no salt added), 1,000 µS/cm, 4,000 µS/cm, and 7,000 µS/cm.
232 These values were chosen, respectively, to represent control conditions, average roadside
233 conditions, maximum roadside conditions, and values exceeding roadside conditions to
234 consider a broad range of exposure scenarios. Embryo clusters were assigned haphazardly to
235 one of four salinity treatments in a 5.6 L container (30.5 x 10 x 20 cm) containing 5 L of
236 assigned treatment solution such that each pond had representative embryos raised in each
237 treatment solution. Containers were arranged randomly across four levels of a shelving unit and
238 were rotated weekly within and between shelves to distribute potential block effects. When
239 tadpoles reached feeding stage, they were fed 5-day food rations containing a 3:1 ratio of rabbit
240 chow to fish food concurrently with water changes. Tadpoles were raised until they reached
241 approximately Gosner stage 35. After recording tadpole developmental stage scores, individuals
242 were euthanized via immersion in buffered Tricaine (2g/L MS222 ethyl 3-aminobenzoate
243 methanesulfonate, Sigma-Aldrich; pH 7.0) and gills were immediately excised and prepped for
244 scanning electron microscopy (SEM). All methods complied with institutional animal care
245 guidelines

246 *Scanning electron microscopy sample preparation*

247 We selected tadpoles haphazardly for SEM, imaging 19 individual tadpoles representing
248 different salt treatments and populations (see Supp Table 1). This sample size was chosen to
249 balance SEM constraints (e.g., costs, sample prep time, personnel time) with study goals.
250 Selected individuals ranged in Gosner developmental stage from 34-37. For each tadpole, the
251 left gill was excised, measured for length using the reticle of a dissecting scope, and
252 immediately transferred to 3% glutaraldehyde in phosphate buffer at 4˚C for 1.5 hours, then

transferred into 1% osmium tetroxide in phosphate buffer for 2 hours at 4˚C. Gills were then dehydrated in a series of graded ethanol steps (30%, 50%, 70%, 80%, 90% and 100%), modified from Brunelli et. al (2004). Gills were dried in a Tousimis Samdri-780 critical point drier and fixed to SEM stubs. Gills were imaged with a Zeiss Sigma VP field emission scanning electron microscope.

Gill Morphology

Images were analyzed using ImageJ software (v. 1.51, Schneider et al. 2012). To describe potential effects of salt on gill morphology, we targeted measuring 12 different traits per gill (Table 1). We measured gill tuft traits (N= 7) corresponding to available surface area (e.g. tuft branch length and width), gill filter traits (N=5) corresponding with surface area available for ion exchange (e.g. internode length), and traits related to filtering efficacy (e.g. internode length and angle). Tuft branch cell attributes were also measured to assess how cell morphology may contribute to ultrastructure (observable through electron microscopy) changes. Each gill was assessed for multiple traits; however, SEM imaging could not guarantee comprehensive coverage of all traits on each gill (see Supplemental Table 1).

For gill tufts, we measured epithelial cell attributes including cell area (C_A) and cell perimeter (C_P) by tracing the perimeter of cells where boundaries were clearly definable, targeting 25 cells per gill (illustrated in Fig. 2a). Cell aspect ratio and circularity were calculated from these values to characterize cell shape. Tuft cell density (T_D) was calculated by tracing clusters of cells within tuft branches and counting the number of cells in each defined area, then computing the value of cell count over area. Tuft branch measurements were obtained by averaging three linear measurements in tuft branch length (T_L) and tuft branch width (T_W), respectively (illustrated in Fig. 3a). We averaged three measurements per trait per branch to account for nonuniform width along branches and imprecise branch origins.

For gill filters, we measured internode distance for both main folds (D_M) and secondary folds (D_S) (Fig. 4a). We also measured angles between main folds (φ_{MM}) and secondary folds (φ_{MS}) (Fig. 4a). Measurements for φ_{MS} angles were measured starting from the ventral end of the main fold (proximal to branchial arch) and tracing the angle of the secondary fold, φ_{MM} angles were measured ventrodorsally. The distance between main folds (D_{MM}) on filter plates (Fig. 4a) was measured by taking the average of three measurements of the distance from a point on the main fold apparatus (corresponding to nodes and points midway between nodes) to the nearest point on an adjacent main fold apparatus.

285

286 *Analysis*

287 To maximize power given our sample size, we composited data into two groups instead of the
288 original four treatment groups – 'high salinity' comprised the three different salt concentrations
289 while 'low salinity' comprised the control group. We used the 'lme4' package (Haubo Bojesen et
290 al., 2017) in RStudio (v. 3.6.2, RStudio Team, 2020) to compose linear mixed effects models
291 analyzing each gill trait in response to salinity. We included gill length and developmental stage
292 as fixed effect covariates because of their potential to influence morphology. In each model,
293 pond and gill identity were included as random effects to account for correlation within ponds
294 and among repeated measurements on each gill. For each trait, we used AIC selection to
295 choose the preferred random effects structure with a delta AIC threshold value of 2. Initial
296 models were fit for AIC selection using restricted maximum likelihood, and selected models for
297 inference were refit with maximum likelihood. *P*-values for fixed effects were based on degrees
298 of freedom calculated with Satterthwaite's approach implemented in the R package
299 'lmerTest' (Haubo Bojesen et al., 2017). We estimated surface area and volume for gill tuft
300 branches by treating them as idealized cylinders and used model estimates for T_L. Because T_W
301 did not vary significantly, the average of T_W estimates was used for surface area and volume
302 estimates. We estimated the filter niche area (i.e., size of spaces within filters) by treating them
303 as rectangles with sides D_M and D_S and used model estimates for D_S. As D_M did not vary
304 significantly, we used the average of D_M model estimates for low and high salinity treatments.

305

306 **Results**

307 Tuft branches were longer in high versus low salinity treatments ($F_{1, 7.4}$ = 8.3, P = 0.022; fig. 3b).
308 Specifically, model estimates for tuft branch length were 31.6 µm for gills in the low salinity
309 treatments compared to 47.2 µm in the high salinity treatments. Thus, gill tuft branch length
310 increased by an estimated 49.5% in tadpoles raised in high salinity conditions. Gill tuft branch
311 width ($F_{1, 9.4}$ = 0.5, P = 0.484) did not vary between salinity treatments. Calculations of branch
312 surface area and volume using these model estimates gave a 41.86% increase in surface area
313 from low salinity to high salinity treatments, but a 49.46% increase in tuft branch volume,
314 reducing the surface area to volume ratio by 5.4% in high salinity treatments.

Traits associated with tuft cells also varied in response to salinity: cell aspect ratio ($F_{1, 294}$ = 15.6, P = 0.001; fig. 2b), cell circularity ($F_{1, 5.0}$ = 13.1, P = 0.0152; fig. 2c) and cell density ($F_{1, 9.9}$ = 7.0, P = 0.025; fig. 2d) each varied in response to salinity. Model estimates for aspect ratio was 1.45 in low salinity treatments versus 1.63 in high salinity treatments, representing an 11.9% increase. Circularity in low salinity was estimated to be 0.611 compared to 0.562 in high salinity, revealing a 7.96% decrease in circularity for high salinity treatments. Cell density was 47.4% higher in high salinity tadpoles, with 0.025 cells per μm^2 compared to 0.017 cells per μm^2 in low salinity treatments. Tuft cell perimeter ($F_{1, 8.0}$ = 1.5, P = 0.260) and tuft cell area ($F_{1, 8.0}$ = 1.0, P = 0.354). No significant variation in any tuft trait occurred in response to Gosner developmental stage or gill length (all P > 0.166).

The distance between gill filter secondary nodes (D_S) varied between low and high salinity treatments ($F_{1, 4.8}$ = 10.3, P = 0.026; fig. 4b). In low salinity treatments, D_S was estimated to be 13.52 µm compared to 22.96 µm for high salinity treatments, representing a 68.52% increase in D_S for tadpoles raised in high salinity. There was marginal support for an effect of salinity on main fold internode distance (D_M) ($F_{1, 4.8}$ = 6.0, P = 0.060; fig. 4c) and distance between main folds (D_{MM}) ($F_{1, 4.0}$ = 5.4, P = 0.081; fig. 4d). Specifically, D_M model estimates were 14.43 µm in low salinity treatments and 21.34 µm in high salinity, representing a 32.36% increase in D_M in high salinity. D_{MM} model estimates were 45.76 µm in low salinity treatments and 79.26 µm in high salinity treatments, representing a 57.74% increase in high salinity. Main fold-main fold angles (φ_{MM}) ($F_{1, 4.3}$ = 4.0, P = 0.111), and main fold-secondary fold angles (φ_{MS}) ($F_{1, 3.9}$ = 0.8, P = 0.431) did not vary significantly between animals raised in low salinity and high salinity conditions. Calculating changes in filter niche area by using model estimates gave a 69.23% increase for filter niche area in high salinity. While neither Gosner developmental stage nor gill length covariates were correlated with filter trait variation in most of these models (D_M, D_S, φ_{MM}, φ_{MS}; P > 0.411), D_{MM} was correlated with gill length ($F_{1, 4.0}$ = 5.4, P > 0.060), increasing 25.9 µm with each 1 mm of gill length.

Discussion

High salinity had numerous effects on tadpole gill morphology. Tuft branch length increased by nearly half while its width was unchanged. Cells on these tufts were more tightly packed together and were less circular, with relatively longer major than minor axes, but cell perimeter and area were unchanged. For gill filters, the distance between nodes was longer, which should result in larger filter size. Together, these results demonstrate that chronic exposure to road salt modifies gill morphology in ways that reduce available surface area to volume ratio and increase

348 the spacing of gill filters. These changes appear likely to compromise the functional capacity of
349 gills for osmoregulation, gas exchange, and foraging.

350 Gill tufts are the primary site of ionoregulation and gas exchange. Increased tuft length (T_L) in
351 the absence of increased width (T_W), strongly suggests that changes in morphology due to salt
352 reduce the available surface area to volume ratio, thus reducing the efficiency and capacity of
353 ion and gas exchange. Indeed, we estimated a 5.4% reduction in surface area to volume ratio
354 for larvae from high salinity treatments. In addition to presumably lowering the efficiency of ion
355 exchange, this change should also reduce the efficiency of gas exchange, which in turn likely
356 exacerbates the already-increased metabolic demands of elevated salinity (Peña-Villalobos et
357 al. 2016). The increase in cell density on tufts was attributable to changes in cell shape, allowing
358 tighter packing of cells on the gill tufts. An increase in cell density could be a response to
359 increase the rate of ion exchange, as no difference in cell area was found in high salinity
360 treatments. While this could offset the reduction in the surface area to volume ratio found in high
361 salinity treatments, a higher cell density is likely to incur a higher energetic cost. However, more
362 information about cell-specific metabolic rates is needed to determine the extent of this tradeoff.

363 Gill filters screen food and particulates out of the water prior to gas exchange at the tufts, and
364 thus play an important role in foraging and feeding (Feder et al. 1984; McIndoe and Smith 1984;
365 Brunelli et al. 2004). Here, filter size appeared to increase in response to salinity, as evidenced
366 by increased length of secondary node distance and (cautiously) the marginal evidence for
367 increased distance between main folds and main fold internode distance. Increased filter size
368 presumably reduces the efficacy of filtering food particles, as more food particles are likely to be
369 flushed out through the operculum instead of being retained for consumption (Seale and
370 Wassersug, 1979). In turn, foraging efficiency should decrease due to high salinity, and this
371 particular change in morphology could bear an energetic cost as larvae might be required to
372 increase foraging efforts. However, this change in filter structure likely increases the available
373 area for ion exchange along the matrix (so-called 'ramifications') of the gill filters. Thus, there
374 might be a tradeoff between foraging efficacy and osmoregulatory capacity.

375 A reduction in the ability of gill filters to both capture food and remove particulates from
376 incoming water before it reaches the tufts may have compounding effects, leading to the widely
377 reported lethal and sublethal consequences of salinity exposure on amphibians. Allowing larger
378 particles to contact and potenitally entangle within the tufts (dowstream of the filters) could
379 reduce the available area for gas exchange. This effect would be magnified by increases in NKA

380 expression in response to salt (Bernabò et al., 2013; Wu et al., 2014) and the associated
381 increase in the metabolic demands of osmoregulation (Peña-Villalobos et al., 2016). When
382 these physiological effects are considered along with observed reductions in foraging activity
383 (Hall et al., 2017), a decrease in the filter's ability to capture food could have substantial impacts
384 on survival. Diminshed feeding capacity coupled with larger, less efficient gill tufts likely
385 constrains larval metabolic resources that are necessary to cope with the osmoregulatory
386 burden of salt-polluted water.

387 It is interesting to consider that even though gill tuft surface area to volume ratio declined in
388 response to high salinity, the length of gill tuft branches and filter secondary folds increased.
389 This pattern of increased size contrasts with other morphological trait responses for amphibians
390 exposed to high salinity. For instance, body length and mass have been shown to decrease in
391 response to salt in numerous studies (e.g., Gomez-Mestre and Tejedo, 2003; Wu and Kam,
392 2009). Thus, the effect of high salinity on amphibian morphology appears to be tissue-specific.
393 Osmoregulatory mechanisms in tadpole gill tissues might play a role in these differences via
394 changes in voltage gradients across membranes. Non-excitable cell depolarization is associated
395 with tissue growth and development (Shi and Borgens, 1995; Reid and Zhao, 2014), and the
396 ionic gradient that tadpoles maintain across gill epithelium for osmoregulatory function creates a
397 voltage gradient that Alvarado and Moody (1970) measured at -5 to -10 mV in pond water,
398 which depolarized as salinity increased to 20mM/L (1,950 μS/cm). While further work is needed
399 to characterize the mechanism behind increased gill tuft and filter size in response to salinity,
400 we are intrigued by the possibility of salinity-induced depolarization contributing to the increases
401 in gill structure size.

402

403 **Acknowledgements**

404 We acknowledge the use of facilities and support (personnel and supplies) from the CT State
405 Colleges and Universities Center for Nanotechnology, Werth Industry Academic Fellowship, and
406 New Haven Innovation Collaborative Undergraduate Research Fellowship Programs. We thank
407 E. Brunelli for providing expertise in amphibian gill anatomy. We are grateful for field and
408 laboratory work by M. Forgione, L. Frymus, J. Priester, F. Senturk, and A. Tucker.

409 **Competing Interests**

410 No competing interests declared

411

412 **Data Availability**

413 All data will be made available in a public repository upon acceptance.

414

415 **References**

416 **Alam, M. R., Sharmin, S., Islam, S. M., Alam, M. A., Ehiguese, F. O., Pattadar, S. N. and**
417 **Shahjahan, M.** (2020). Salinity intrusion affects early development of freshwater aquaculture
418 species pabda, *Ompok pabda*. *Aquac. Reports.* **18,** 100476.

419 **Albecker, M.A. and McCoy, M.W.** (2017). Adaptive responses to salinity stress across multiple
420 life stages in anuran amphibians. *Front. Zool*. **14**, 1–16.

421 **Alexander, L.G., Lailvaux, S.P., Pechmann, J.H.K. and DeVries, P.J.** (2012). Effects of
422 Salinity on Early Life Stages of the Gulf Coast Toad, Incilius nebulifer (Anura: Bufonidae).
423 *Copeia*. **2012,** 106–114.

424 **Alvarado, R.H. and Moody, A.** (1970). Sodium and chloride transport in tadpoles of the bullfrog
425 Rana catesbeiana. *Am. J. Physiol*. **218**, 1510–1516.

426 **Bernabò, I., Bonacci, A., Coscarelli, F., Tripepi, M. and Brunelli, E.** (2013). Effects of salinity
427 stress on Bufo balearicus and Bufo bufo tadpoles : Tolerance , morphological gill alterations and
428 Na + / K + -ATPase localization. *Aquat. Toxicol*. **132–133**, 119–133.

429 **Boonkoom, V. and Alvarado, R. H.** (1971). Adenosinetriphosphatase activity in gills of larval
430 *Rana catesbeiana*. *Am. J. Physiol.* **220(6)**, 1820–1824.

431 **Brady, S.P.** (2012). Road to evolution? Local adaptation to road adjacency in an amphibian
432 (*Ambystoma maculatum*). *Sci. Rep.* **2,** 1–5.

433 **Brady, S.P.** (2013). Microgeographic maladaptive performance and deme depression in
434 response to roads and runoff. *PeerJ*. **2013,** e163.

435 **Brady, S. P.** (2017) Environmental exposure does not explain putative maladaptation in road-

436 adjacent populations. *Oecologia*. **184(4)**, 931–942.

437 **Brady, S.P., Bolnick, D.I., Barrett, R.D.H., Chapman, L., Crispo, E., Derry, A.M., Eckert,**
438 **C.G., Fraser, D.J., Fussmann, G.F., Gonzalez, A., et al.** (2019). Understanding maladaptation
439 by uniting ecological and evolutionary perspectives. *Am. Nat.* **194**, 495–515.

440 **Bridgeman, T.B., Wallace, C.D., Carter, G.S., Carvajal, R., Schiesari, L.C., Aslam, S.,**
441 **Cloyd, E., Elder, D., Field, A., Schulz, K.L., et al.** (2000). A limnological survey of third sister
442 lake, michigan with historical comparisons. *Lake Reserv. Manag.* **16**, 253–267.

443 **Brunelli E., Perrotta E. and Tripepi, S.** (2004). Ultrastructure and development of the gills in
444 *Rana dalmatina* (Amphibia, Anura). *Zoomorphology*. **123**, 203–211.

445 **Campbell, C.R., Voyles, J., Cook, D.I. and Dinudom, A.** (2012). Frog skin epithelium:
446 Electrolyte transport and chytridiomycosis. *Int. J. Biochem. Cell Biol.* **44,** 431–434.

447 **Castillo, A.M., Sharpe, D.M.T., Ghalambor, C.K. and De León, L.F.** (2018). Exploring the
448 effects of salinization on trophic diversity in freshwater ecosystems: a quantitative review.
449 *Hydrobiologia* **807**, 1–17.

450 **Chinathamby, K., Reina, R. D., Bailey, P. C. E. and Lees, B. K.** (2006). Effects of salinity on
451 the survival, growth and development of tadpoles of the brown tree frog, *Litoria ewingii*. *Aust. J.*
452 *Zool*. **54**, 97.

453 **Dananay, K. L., Krynak, K. L., Krynak, T. J. and Benard, M. F.** (2015). Legacy of road salt:
454 Apparent positive larval effects counteracted by negative postmetamorphic effects in wood
455 frogs. Environ. *Toxicol. Chem.* **34**, 2417–2424.

456 **Denoël, M., Bichot, M., Ficetola, G.F., Delcourt, J., Ylieff, M., Kestemont, P. and Poncin, P.** (2010).
457 Cumulative effects of road de-icing salt on amphibian behavior. *Aquatic Toxicology*, **99(2)**, 275-280.

458 **Dietz, T. H. and Alvarado, R. H.** (1974). Na and Cl transport across gill chamber epithelium of
459 *Rana catesbeiana* tadpoles. *American Journal of Physiology*, **226(4)**. 764–770.

460 **Dugan, H. A., Bartlett, S. L., Burke, S. M., Doubek, J. P., Krivak-Tetley, F. E., Skaff, N. K.,**
461 **Summers, J. C., Farrell, K. J., McCullough, I. M., Morales-Williams, A. M., et al.** (2017).
462 Salting our freshwater lakes. *Proc. Natl. Acad. Sci. U. S. A.* **114**, 4453–4458.

463 **Faulkner, P. C., Hala, D., Rahman, M. S. and Petersen, L. H.** (2019). Short-term exposure to

12‰ brackish water has significant effects on the endocrine physiology of juvenile American alligator (*Alligator mississippiensis*). *Comp. Biochem. Physiol. -Part A Mol. Integr. Physiol.* **236**, 110531.

Feder, M. E., Seale, D. B., Boraas, M. E., Wassersug, R. J. and Gibbs, A. G. (1984). Functional conflicts between feeding and gas exchange in suspension-feeding tadpoles, *Xenopus laevis*. *J. Exp. Biol.* **110**, 91-98.

Findlay, S. E. G. and Kelly, V. R. (2011). Emerging indirect and long-term road salt effects on ecosystems. Ann. *N.Y. Acad. Sci*. **1223**, 58-68.

Gibbons, T. C., McBryan, T. L. and Schulte, P. M. (2018). Interactive effects of salinity and temperature acclimation on gill morphology and gene expression in threespine stickleback. *Comparative Biochemistry and Physiology -Part A : Molecular and Integrative Physiology*. **221**, 55–62.

Gomez-Mestre, I. and Tejedo, M. (2003). Local adaptation of an anuran amphibian to osmotically stressful environments. *Evolution*. **57**, 1889–1899.

Gomez-Mestre, I., Tejedo, M., Ramayo, E., Estepa, J. and Luisa, M. (2004). Developmental Alterations and Osmoregulatory Physiology of a Larval Anuran under Osmotic Stress. *Physiol. Biochem. Zoo.* **77(2)**, 267-274

Gordon, M. S. and Tucker, V. A. (1965). Osmotic regulation in the tadpoles of the crab eating frog (*Rana cancrivora*). *J. Exp. Bio.* **42**, 437-445.

Gosner, K. L. (1960) A simplified table for staging anuran embryos and larvae with notes oniIdentification. *Herpetologica.* **16(3)**, 183–190.

Gutierrez, M. F., Tavşanoğlu, Ü. N., Vidal, N., Yu, J., Teixeira-de Mello, F., Çakiroglu, A. I., He, H., Liu, Z. and Jeppesen, E. (2018). Salinity shapes zooplankton communities and functional diversity and has complex effects on size structure in lakes. *Hydrobiologia.* **813(1)**, 237–255.

Green D. M., Weir L. A., Casper G. S. and Lannoo M. J. (2014). *North American Amphibians: Distribution and Diversity*. University of California Press, Berkeley, California.

Green, D. M., Lannoo, M.J., Lesbarrères, D. and Muths, E. (2020). Amphibian population declines: 30 years of progress in confronting a complex problem. *Herpetologica*. **76(2)**, 97–100.

Hall, E. M., Brady, S. P., Mattheus, N. M., Earley, R. L., Diamond, M. and Crespi, E. J.

(2017). Physiological consequences of exposure to salinized roadside ponds on wood frog larvae and adults. *Bio. Conserv.* **208**, 98-106.

Haubo Bojesen, R., Kuznetsova, A., Brockhoff, P. B. and B. Christensen, R. H. (2017). General rights lmerTest Package: Tests in Linear Mixed Effects Models lmerTest Package: Tests in Linear Mixed Effects Models. *orbit.dtu.dk* 82. doi:10.18637/jss.v082.i13.

Hintz, W. D., Mattes, B. M., Schuler, M. S., Jones, D. K., Stoler, A. B., Lind, L. and Relyea, R. A. (2017). Salinization triggers a trophic cascade in experimental freshwater communities with varying food-chain length. *Ecological Applications*. **27(3)**, 833–844.

Hintz, W.D. and Relyea, R.A. (2019). A review of the species, community, and ecosystem impacts of road salt salinisation in fresh waters. *Freshw. Biol.* **64**, 1081–1097.

Hiroi, J., Kaneko, T. and Tanaka, M. (1999). Sequential changes in chloride cell morphology. *J. Exp. Bio.* **202**, 3485-3495.

Hopkins, G. R. and Brodie, E. D. (2015). Occurrence of Amphibians in Saline Habitats: A Review and Evolutionary Perspective. *Herpetol. Monogr.* **29**,1–27.

Hopkins, G. R., French, S. S. and Brodie, E. D. (2013). Increased frequency and severity of developmental deformities in rough-skinned newt (*Taricha granulosa*) embryos exposed to road deicing salts (NaCl & MgCl2). *Environ. Pollut.* **173**, 264–269.

Hsu, W. T., Wu, C. S., Lai, J. C., Chia, Y. K., Hsu, C. H. and Kam, Y. C. (2012) Salinity acclimation affects survival and metamorphosis of crab-eating frog tadpoles. *Herpetologica***.** **68(1)**, 14–21.

Hwang, P. P. and Lee, T. H. (2007). New insights into fish ion regulation and mitochondrion-rich cells. *Comparative Biochemistry and Physiology - A Molecular and Integrative Physiology*. **148(3)**, 479–497.

Judd, K. E., Adams, H. E., Bosch, N. S., Kostrzewski, J. M., Scott, C. E., Schultz, B. M., Wang, D. H. and Kling, G. W. (2005). A case history: Effects of mixing regime on nutrient dynamics and community structure in third sister lake, Michigan during late winter and early spring 2003. *Lake Reserv. Manag.* **21**, 316–329.

Karraker, N. E., Gibbs, J. P. and Vonesh, J. R. (2008). Impacts of road deicing salt on the demography of vernal pool-breeding amphibians. *Ecol. Appl.* **18**, 724–734.

Kaushal, S. S., Groffman, P. M., Likens, G. E., Belt, K. T., Stack, W. P., Kelly, V. R., Band, L. E. and Fisher, G. T. (2005). Increased salinization of fresh water in the northeastern United States. *Proc. Natl. Acad. Sci. U.S.A.* **102**, 13517-13520.

Lauer, N. E., Harkness, J. S. and Vengosh, A. (2016) Brine Spills Associated with Unconventional Oil Development in North Dakota. *Env. Sci. Technol.* **50**, 5389-5397.

Mahrosh, U., Kleiven, M., Meland, S., Rosseland, B. O., Salbu, B. and Teien, H. C. (2014). Toxicity of road deicing salt (NaCl) and copper (Cu) to fertilization and early developmental stages of Atlantic salmon (*Salmo salar*). *J. Hazard. Mater.* **280**, 331–339.

Maloney K. O., Baruch-Mordo S., Patterson L. A., Nicot J. P., Entrekin S. A., Fargione J. E., Kiesecker J. M., Konschnik K. E., Ryan J. N., Trainor A. M., et al. (2017). Unconventional oil and gas spills: Materials, volumes, and risks to surface waters in four states of the U.S. *Sci. Total Environ.* **581–582**, 369–377.

McIndoe, R. and Smith, D. G. (1984). Functional anatomy of the internal gills of the tadpole of *Litoria ewingii* (Anura, Hylidae). *Zoomorphology.* **104**, 280–291.

Merrick, A. M. and Searle, C. L. (2019). Combined effects of salinity and infectious disease on *Daphnia dentifera* at multiple scales. *Freshw. Biol.* **64**, 601–607.

Van Meter, R. J. and Swan, C.M. (2014). Road Salts as Environmental Constraints in Urban Pond Food Webs. *PLoS One* **9**, e90168.

Park, J.-K. and Do, Y. (2020). Physiological Response of *Pelophylax nigromaculatus* Adults to Salinity Exposure. *Animals*. **10(9)**, 1698.

Peña-Villalobos, I., Narváez, C. and Sabat, P. (2016). Metabolic cost of osmoregulation in a hypertonic environment in the invasive African clawed frog *Xenopus laevis. Biol. Open* **5**, 955–961.

Pivovarov, A. S., Calahorro, F. and Walker, R. J.. (2019). Na+/K+-pump and neurotransmitter membrane receptors. *Invertebr. Neurosci.* **19**, 1-16.

Pough, F. H. (2007). Amphibian Biology and Husbandry. *ILAR J.* **48**, 203–213.

Reid, B. and Zhao, M. (2014). The electrical response to injury : molecular mechanisms and wound healing. *Adv. Wound Care.* **3**, 184–201.

Richburg, J. A., Patterson, W. A. and Lowenstein, F. (2001). Effects of road salt and phragmites Australis invasion on the vegetation of a western Massachusetts calcareous lake-basin fen. *Wetlands.* **21**, 247–255.

RStudio Team. (2020). RStudio: Integrated Development for R. RStudio, PBC, Boston, MA. *http://www.rstudio.com/*.

Sanzo, D. and Hecnar, S. J. (2006). Effects of road de-icing salt (NaCl) on larval wood frogs (*Rana sylvatica*). *Environ. Pollut.* **140**, 247–256.

Schuler, M. S., Hintz, W. D., Jones, D. K., Lind, L. A., Mattes, B. M., Stoler, A. B., Sudol, K. A. and Relyea, R. A. (2017). How common road salts and organic additives alter freshwater food webs: in search of safer alternatives. *J. Appl. Ecol.* **54**, 1353–1361.

Seale, D.B., and Wassersug, R. J. (1979). Suspension feeding dynamics of anuran larvae related to their functional morphology. *Oecologia.* **39**, 259–272.

Semlitsch, R. D., and Skelly, D. K. (2007). Ecology and Conservation of Pool-Breeding Amphibians. In *Science and Conservation of Vernal Pools in Northeastern North America*. (ed. A. Calhoun and P. deMaynadier). pp. 127-147. Boca Raton: CRC Press.

Shi, R. and Borgens, R. B. (1995). Three-Dimensional Gradients of Voltage During Development of the Nervous System as Invisible Coordinates for the Establishment of Embryonic Pattern. *Dev. Dyn.* **202**, 110-114.

Skou, J. C. (1957). The influence of some cations on an adenosine triphosphatase from peripheral nerves. *BBA - Biochem. Biophys. Acta* **23**, 394–401.

Squires, Z. E., Bailey, P. C. E., Reina, R. D. and Wong, B. B. M. (2008). Environmental deterioration increases tadpole vulnerability to predation. *Biol. Lett.* **4**, 392–394.

Uchida, K., Kaneko, T., Yamauchi, K. and Hirano, T. (1996). Morphometrical analysis chloride cell activity in the gill filaments and lamellae and changes in Na+, K+-ATPase activity during seawater adaptation in chum salmon fry. *Journal of Experimental Zoology*, **276(3)**, 193-200.

Uchiyama, M. and Yoshizawa, H. (1992). Salinity tolerance and structure of external and internal gills in tadpoles of the crab-eating frog, *Rana cancrivora*. *Cell Tissue Res*. **267**, 35–44.

Ultsch, G. R., Bradford, D. F. and Freda, J. (1999). *Tadpoles: the biology of anuran larvae*.

580 Chicago: University of Chicago Press.

581 **Venâncio, C., Castro, B. B., Ribeiro, R., Antunes, S. C. and Lopes, I.** (2019). Sensitivity to
582 salinization and acclimation potential of amphibian (*Pelophylax perezi*) and fish (*Lepomis*
583 *gibbosus*) models. *Ecotoxical. Env. Saf.* **172**, 348-355.

584 **Vences, M. and Köhler, J.** (2008). Global diversity of amphibians (Amphibia) in freshwater.
585 *Hydrobiologia* **595**, 569–580.

586 **Wilson, J. M.** (2011). Role of the gills | Morphology of Branchial Ionocytes. In *Encyclopedia of*
587 *Fish Physiology. Vol. 2.* (ed. A. P. Farrell). pp. 1381–1388. Oxford, UK: Elsevier Inc.

588 **Wu, C. S. and Kam, Y. C.** (2009). Effects of salinity on the survival, growth, development, and
589 metamorphosis of *Fejervarya limnocharis* tadpoles living in brackish water. *Zoolog. Sci.* **26**,
590 476–482.

591 **Wu, C. S., Yang, W K ., Lee, T. H., Gomez-Mestre, I. and Kam, Y.C.** (2014). Salinity
592 acclimation enhances salinity tolerance in tadpoles living in brackish water through increased
593 Na+, K+-ATPase expression. *J. Exp. Zool. Part A Ecol. Genet. Physiol.* **321**, 57–64.

594

595

596

597

598

599

600

601

602

603

Figures

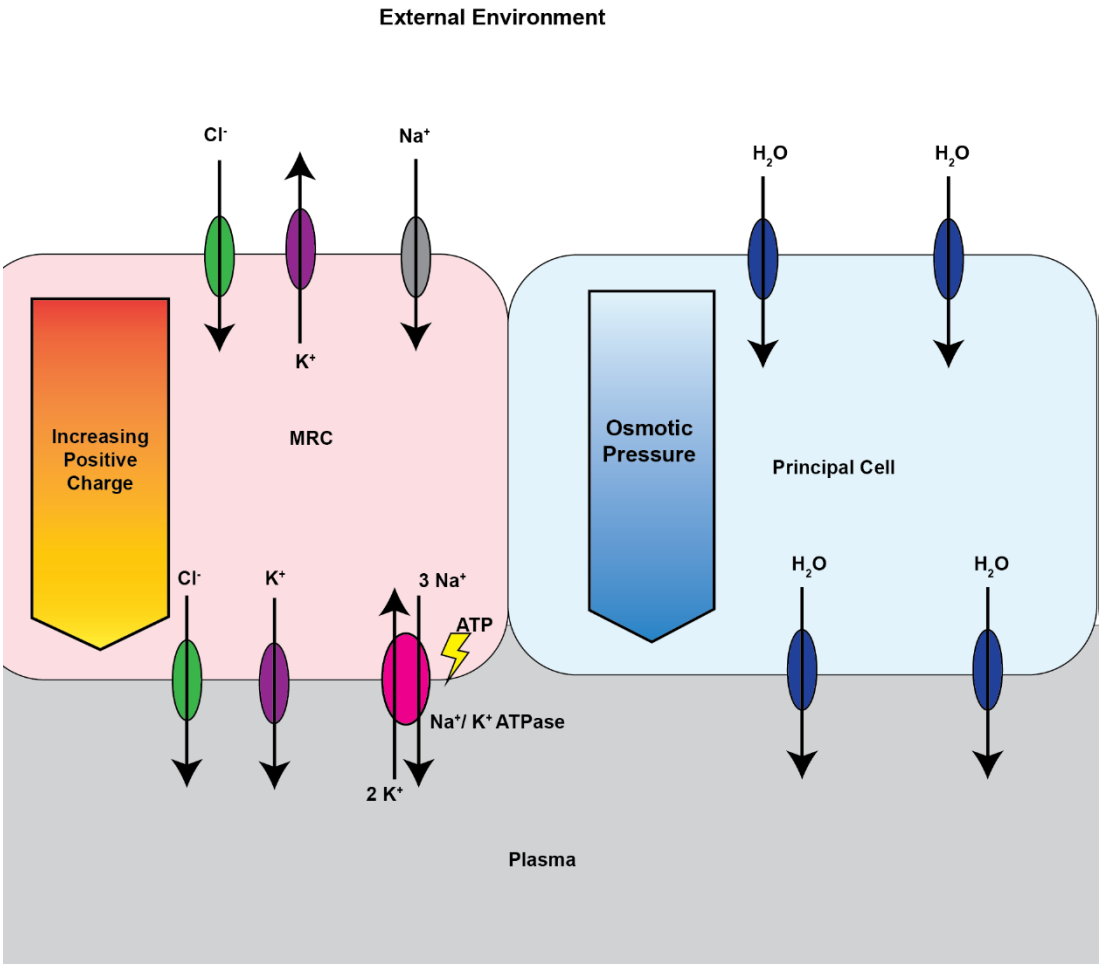

Figure 1. Ionic and Osmotic Control of Osmoregulation Across Gill Epithelium. Mitochondria rich cells (MRC) create a gradient of increasing positive charge through the action of Na^+/K^+ ATPase (NKA) pumps in the basal cell membrane. 3 Na^+ ions are actively pumped out of the cell and 2 K^+ ions are pumped in for every molecule of ATP. This creates a chemical gradient for Na^+ to be drawn into the cytosol through passive Na^+ channels. K^+ is present in higher concentrations inside the cell and so passively exits through K^+ channels into the plasma or the external environment. This high concentration of positive ions in the plasma generates a voltage gradient that allows Cl^- from the environment to pass through the cytosol into the plasma. The osmolality of the plasma is thus increased and aquaporins present in principle cells allow the passive diffusion of water.

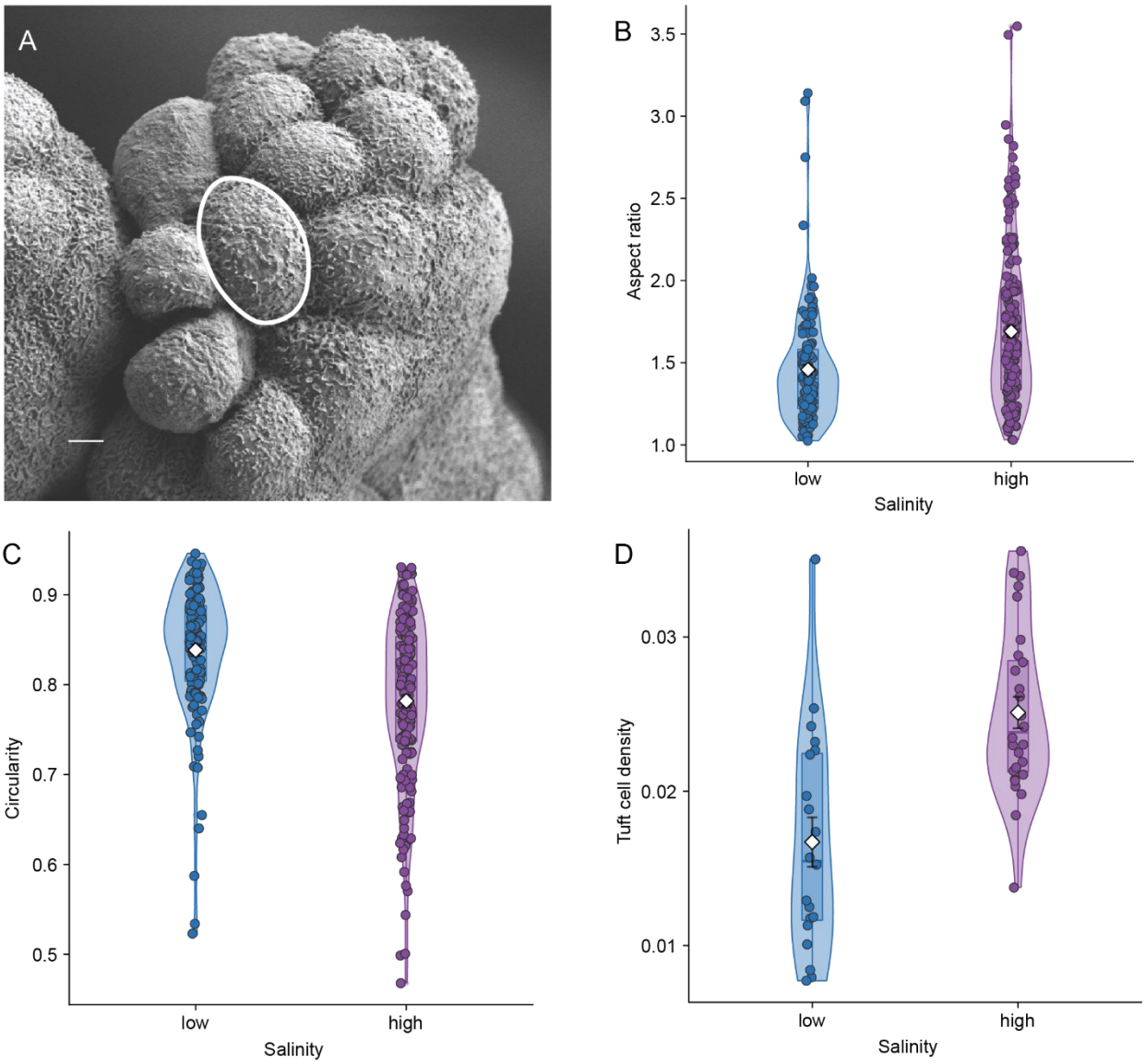

Figure 2. Variation in Tuft Branch Cell Shape and Density. Gill tuft branch at 7000x magnification (A) with a tuft cell circled in white. Scale bar, 2 μm. Cell shape was measured by tracing cells with well-defined borders and measuring area, perimeter, aspect ratio (B), and circularity (C). Tuft cell density (D) was obtained by tracing cell branches and counting cells within measured area. Points represent individual measurements and were jittered to reduce overlap; violin plots show density distributions, overlayed with a boxplot. Means with SE bars are shown with white diamond. Aspect ratio increased with salinity and circularity decreased. Altered cell shape in high salt treatments coincided with higher cell density.

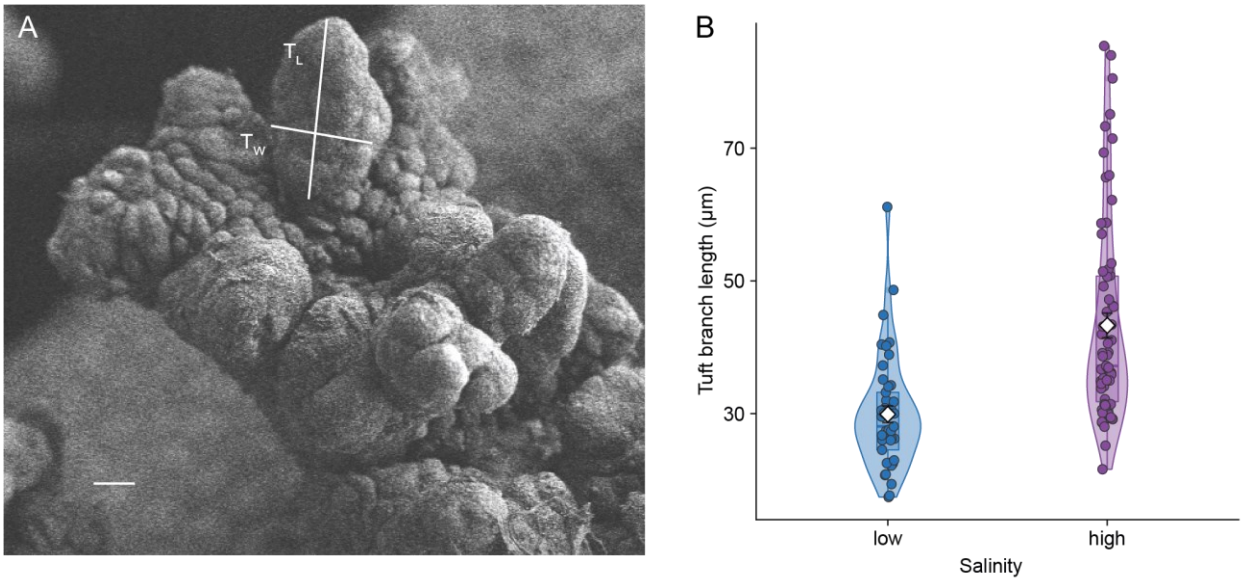

Figure 3. Gill Tuft Branch Variation in response to salt. Gill tuft (A) with representative tuft branch length (T_L) and tuft branch width (T_W) depicted in white. Scale bar, 10 µm. Each datapoint for tuft dimensions is the average of three measurements taken per trait per tuft branch. Tuft branches are nonuniform in width, measurements were taken at towards the base, midsection, and apex accordingly. Tuft branch length (B) was averaged due to the boundary of the tuft branch at its base being imprecise. Points represent individual measurements and were jittered to reduce overlap; violin plots show density distributions, overlayed with a boxplot. Means with SE bars are shown with white diamond. T_L increased in response to salt, was less densely distributed around the mean and had a wider range of values. T_W was not found to vary in response to salt.

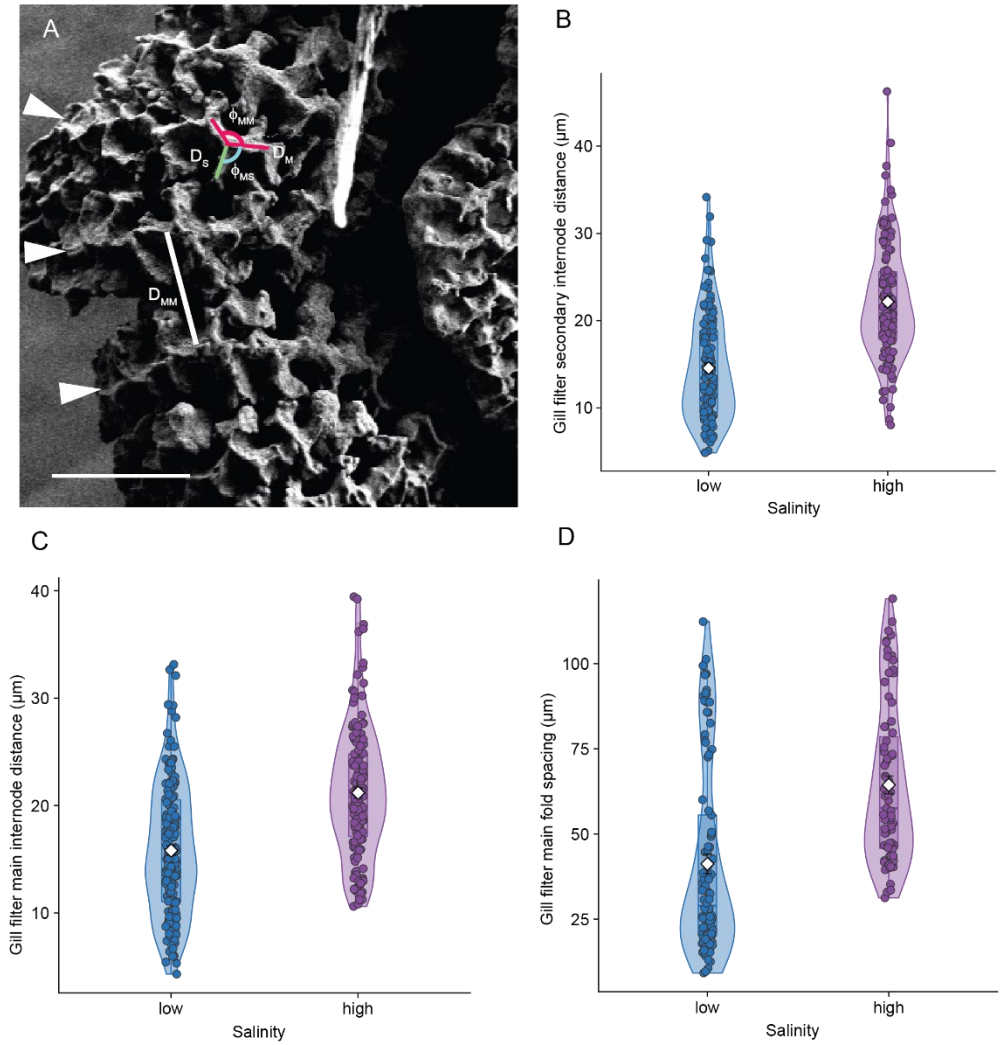

Figure 4. Gill Filter Fold Variation in Response to Salt. Gill plate with filters of epithelial tissue exposed (A). Scale bar, 100 µm. Main folds (arrows) run ventrodorsally along the gill plate (right to left in image above). Representative main internode distances (D_M) are depicted in red, and main fold angle (φ_{MM}) is represented by the red arc between lines. A representative secondary internode distance (D_S) is depicted in green, and the main fold-secondary fold angle (φ_{MS}) is depicted by the blue arc. A representative measurement of the distance between main fold rows (D_{MM}) is shown in white. D_S (B), D_M (C), and D_{MM} (D) distances. Points represent individual measurements and were jittered to reduce overlap; violin plots show density distributions, overlayed with a boxplot. Means with SE bars are shown with white diamond. D_S increased in response to salinity.

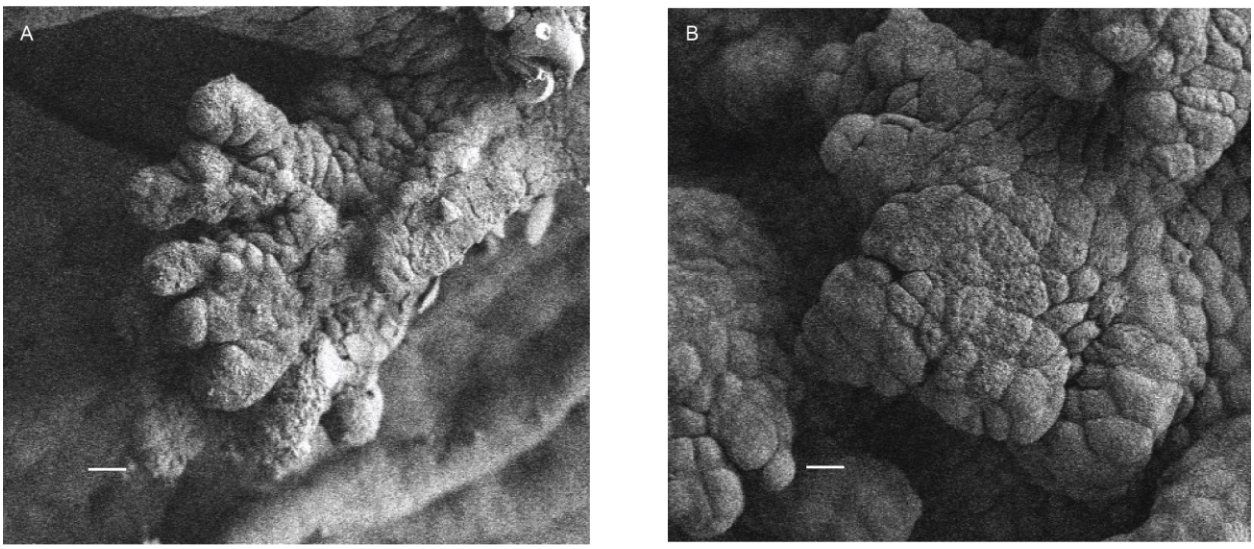

Figure 5. Comparison of Gill Tufts from Control and Salt Treatments. (A) Tufts from animals in control treatments were contracted relative to the fuller appearance of (B) tufts from salt treatments. Scale bars,10 µm.

Gill Trait	Description
Gill Tufts	
Branch Length (T_L)	Length of tuft branch from base of branch to tip. Each datapoint for this trait in our study is the average of three such measurements per branch to account for imprecise branch origins.
Branch Width (T_W)	Width of tuft branch. Each datapoint for this trait in our study is the average of three such measurements per branch to account for tapering of branches from broader bases to narrower termini.
Cell Area	Area of gill tuft cells as defined by cell borders at apical epithelium.
Cell Perimeter	Perimeter of gill tuft cells as defined by cell borders at apical epithelium.
Cell Aspect Ratio	Ratio of the major axis, or longest diameter through the cell, to the minor axis, or shortest diameter through the cell.
Cell Circularity	A measure of how closely the perimeter of the cell describes a circle. Given by the formula $4\pi \frac{Area\ of\ ellipse}{perimeter\ of\ ellipse^2}$ A circularity value of 1 denotes a perfect circle.
Cell Density	The number of cells present within tuft cell branches.
Gill Filters	
Main Fold Spacing	The distance between rows of main folds. Multiple measures were taken between folds to account for differences arising from the zigzagging morphology of gill filter folds.
Main Fold Internode Distance	The distance between points in main folds where either the main fold changed direction, a secondary fold branched from the main fold, or the main fold terminated.
Main Fold to Main Fold Angle	The angle described by two adjacent sections of main fold, joined by a node, that do not lie on the same line
Secondary Fold Internode Distance	The distance between points on secondary folds where either the secondary node joined the main fold, changed direction, a tertiary fold branched from the secondary fold, or the secondary fold terminated.
Main Fold to Secondary Fold Angle	The angle described by two adjacent sections of main and secondary folds of the gill filter. Angles were always measured from the ventral side of the main fold onto the secondary fold.

Table 1. Description of gill traits measured in response to salinity.